Građevinski materijali i konstrukcije
Building Materials and Structures
journal homepage: www.buildingmaterialsstructures.com

https://doi.org/10.5937/GRMK2600002C

Original scientific paper

Low-carbon cementitious material from municipal solid waste incineration bottom ash for street furniture and outdoor paving: A circular economy perspective

Fabian Cuspoca[1,2], Jofre Mañosa[2], Joan Ramon Rosell[1], Gerard Faneca[3], Josep Maria Chimenos[*2]

[1] Department of Architectural Technology, Universitat Politècnica de Catalunya, Doctor Marañón, 44-50, 08028 Barcelona, Spain
[2] DIOPMA Research Group, Materials Science and Physical Chemistry, Universitat de Barcelona, Martí i Franqués 1, 08028 Barcelona, Spain
[3] Escofet 1886 Ltd., La Torre Montserrat Industrial Park 162, 08760 Martorell, Spain

Article history
Received: 28 November 2025
Received in revised form: 09 January 2026
Accepted: 20 January 2026
Available online: 16 February 2026

Keywords
Alternative cementitious materials,
weathered bottom ash,
circular economy,
alkaline activated binders,
plasticizers for alternative cement

ABSTRACT

This study investigates the feasibility of employing municipal solid waste incineration bottom ash (WBA) as the sole precursor for producing alkali-activated binders (AA-WBA), with the aim of developing low-carbon mortars and concretes for non-structural urban applications within a circular-economy framework. The precursor, originally in the 8-30 mm particle-size fraction reported in previous studies, was milled to obtain material below 125 µm. A series of activation conditions was examined by varying the NaOH concentration, the NaOH-to-sodium-silicate ratio, and the liquid-to-solid ratio, together with three precursor particle-size ranges (≤63 µm, 90-100 µm, and 100-125 µm). The optimal formulation (1:4/0.6/4 M; 90-100 µm) achieved satisfactory mechanical performance in paste form and developed a dense microstructure characterised by the formation of C-(A)-S-H/N-A-S-H gels, as evidenced by TGA, FT-IR, and SEM analyses. As a proof of concept, this binder was used to manufacture a full-scale concrete pedestrian paving element, which exhibited adequate mechanical performance for outdoor pedestrian use at 28 days. Leaching and ecotoxicity tests indicated low metal release and no significant toxic effects, thereby demonstrating the environmental safety of the material and its potential contribution to more sustainable construction systems.

1 Introduction

Alkali-activated cements offer a lower environmental-impact alternative to conventional cement production. As a result, there is growing interest within the construction sector in materials capable of partially or fully replacing Portland cement (OPC), the manufacture of which is associated with substantial global CO_2 emissions and high primary energy demand.

In the precast sector, particularly in the manufacture of street furniture, outdoor paving units and other non-structural components, the use of municipal solid waste incineration bottom ash (WBA) as a precursor in alkali-activated cements (AA-WBA) promotes a more sustainable production cycle, sourcing raw materials directly from citizen-generated waste. This approach is feasible because incineration is widely regarded as an effective strategy for managing the growing volume of municipal solid waste [1].

The study is framed within the principles of the circular economy, emphasising their relevance in reducing the carbon footprint associated with both binder production and use. This approach not only enhances the sustainability of cementitious formulations but also valorises waste materials and optimises their management, thereby contributing to a process fully aligned with circular-economy objectives.

The literature review indicates that, although several attempts have been made to optimise AA-WBA systems, studies focusing exclusively on the activation of WBA remain limited [2]. Nevertheless, based on the behaviour reported in previous studies [3–7] and preliminary findings from other authors, there is significant potential to improve the performance of AA-WBA produced solely from WBA. This knowledge gap provides a clear opportunity to further investigate the activation mechanisms and optimise the resulting material properties.

WBA exhibits a wide particle-size distribution [8]. The finer fractions contain the majority of soluble salts and potentially leachable heavy metals (and metalloids), whereas the coarser fractions are predominantly composed of ceramics and glass. Natural weathering over 2-3 months outdoors has been shown to significantly reduce the leaching potential; consequently, in most European countries, WBA is currently classified as non-hazardous waste [9,10]. However, information on the mechanical performance and

* Corresponding author:
E-mail address: chimenos@ub.edu

durability of concretes produced with alkali-activated cements remains limited, despite their previous use in various applications. This gap underscores the need to translate laboratory findings into potential industrial-scale applications, particularly when using WBA as the primary precursor for non-structural components.

Considering environmental criteria and the goal of maximising WBA recovery, the 8-30 mm fraction, also characterized by the highest SiO_2 content [11], has been identified as the most suitable for alkaline activation. During the material preparation stage, and in order to evaluate the mechanical performance of the binder (AA-WBA paste) formulated exclusively from WBA, this fraction was milled to produce particle sizes ≤125 µm, following procedures reported in previous studies [12]. However, it is to be expected that particles within this powdered WBA will display heterogeneous reactivity as precursors during alkaline activation. Therefore, it is anticipated that finer particles generally enhance dissolution kinetics and promote the formation of reaction products, which improves mechanical performance. Furthermore, the mineralogical composition of the particles plays a critical role, as more fragile phases tend to concentrate in the finer fractions, thereby increasing the availability of reactive species such as SiO_2 and Al_2O_3. Nevertheless, excessive grinding raises energy consumption and may compromise industrial feasibility. This variability in particle behavior provides an opportunity to evaluate the balance between chemical reactivity, mechanical strength and processing efficiency.

Using the powdered 8-30 mm WBA fraction, the study aims to evaluate the mechanical behavior (compressive strength) of AA-WBA pastes across three particle-size ranges: ≤63 µm, 90-100 µm, and 100-125 µm. The fraction exhibiting the best mechanical performance was subsequently employed in a proof-of-concept test aimed at evaluating potential industrial-scale application, yielding satisfactory results.

2 Materials and methods

The powdered WBA sample was supplied by Escofet S.A., a Barcelona-based company specializing in the design and industrial production of urban furniture and paving elements. The sample was originally obtained from a local waste-to-energy facility, where it was generated during the combustion of municipal solid waste at approximately 950 °C. This was subsequently conditioned to recover valuable materials [4,8] using magnetic and eddy-current separators. The remaining mineral fraction was stored outdoors for 2-3 months to allow chemical stabilization [13], after which the stabilised bottom ash underwent selection, screening and final grinding. Figure 1 presents the processing route, through which an initial 40-tonne batch of stabilised WBA was treated. During the screening stage, approximately 6 tonnes were recovered within the 8-30 mm particle-size fraction. This range was selected because previous studies [3] have reported that the highest SiO_2 availability occurs in fractions larger than 8 mm. In addition, this fraction is less contaminated and contains lower amounts of metallic aluminium, thereby reducing hydrogen generation compared with other fractions studied previously [12]. Once this fraction had been obtained, it was subjected to a grinding process to reduce the particle size to below 1 mm. Prior to undertaking the secondary grinding stage, a crucial step was performed to remove any remaining metallic impurities that could interfere with both the grinding operation and the final properties of the cementitious material. The conditioned material was then subjected to fine grinding in a ball mill, enabling a particle size of less than 125 µm to be achieved. Table 1 presents the elemental composition of the WBA, determined by X-ray fluorescence (XRF) using a Bruker S2 PUMA Light Element Energy Dispersive X-ray Fluorescence Spectroscopy. The results indicate a high proportion of SiO_2 (46.61%) and CaO (27.74%), both of which are essential for the formation of C-A-S-H and (C,N)-A-S-H gels during alkaline activation.

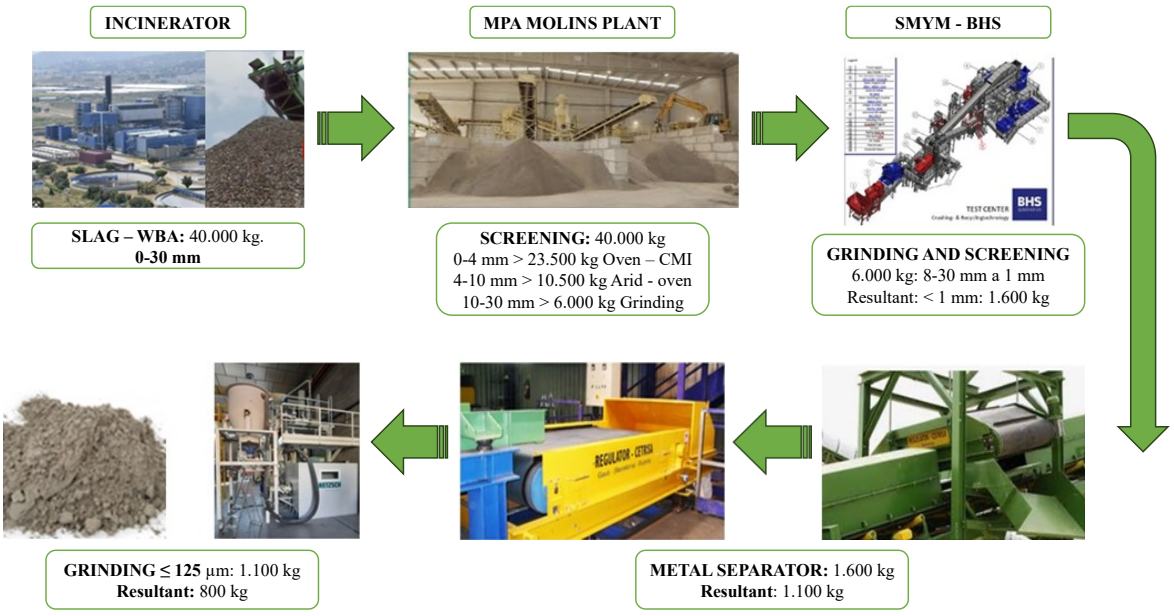

Figure 1. Process of conditioning WBA as a precursor material for alcaline-activated binders

Table 1. Elemental oxide composition of powdered WBA

Major elements	(wt.%)	Minor and traces elements	(wt.%)
SiO_2	48.61	PbO	0.09
CaO	24.74	MnO	0.09
Al_2O_3	9.23	ZrO_2	0.09
Fe_2O_3	4.31	Sc_2O_3	0.08
Na_2O	4.15	Cr_2O_3	0.07
SO_3	2.45	BaO	0.06
MgO	2.32	SrO	0.06
K_2O	1.44	SnO_2	0.02
P_2O_5	0.76	NiO	< 0.01
TiO_2	0.59	Rb_2O	< 0.01
Cl	0.5	HfO_2	< 0.01
ZnO	0.19	MoO_3	< 0.01
CuO	0.12	Br	< 0.01
LOI (1050°C)	9.36		

This powdered WBA exhibits a density of 2.79 g·cm^{-3}, a specific surface area of 4.08 m^2·g^{-1}, and an average adsorption pore width of 20.98 Å. The particle size distribution (PSD) is presented in Figure 2. The analyses were performed using a Beckman Coulter LS13320 operating in micro-liquid mode with ethanol as the dispersant. Crystalline phases were identified by X-ray diffraction (XRD) using a PANalytical X'Pert PRO MPD diffractometer configured in Bragg-Brentano θ/θ geometry with a 240 mm radius. As shown in Figure 3, the material contains numerous mineral phases and a significant fraction of amorphous phases, as evidenced by the angular range from 20 to 35° (2θ).

For the alkaline activation, a mixture of sodium silicate (Na_2SiO_3) and sodium hydroxide (NaOH) was used. The sodium silicate (waterglass, WG) employed was a commercial solution supplied by Sharlab Laboratories, with a density of 1.37 g·cm^{-3}, complete miscibility in water at 20 °C, and a pH of 11-11.5.

2.1 Specimen preparation

All specimens were prepared in 25 mm cubic moulds. For each formulation in the first test series, six specimens were produced for 28-day compressive strength testing using an Incotecnic Multi R-1 universal testing machine, applying a loading rate of 240 kg·s^{-1} in accordance with UNE 196-1 [13]. The specimens were cured in a humid environment. They were placed in resealable bags containing a small water reservoir for the first three days, then demoulded and maintained under the same conditions at 23 ± 1 °C and 95 ± 5% relative humidity . The formulations varied by changing the NaOH:WG ratio, activator-to-precursor ratio (L/S), and the molarity of the NaOH solution (4M, 6M, 8M, and 10M), as summarised in Table 2. Mixing was carried out in a Labbox OS40-series mixer. During the first 2 minutes at 470 rpm, the activator blend was gradually added to the powdered WBA precursor, followed by a further 3 minutes of mixing at 760 rpm [12]. The mixtures were then discharged, vibrated, and cast into the moulds.

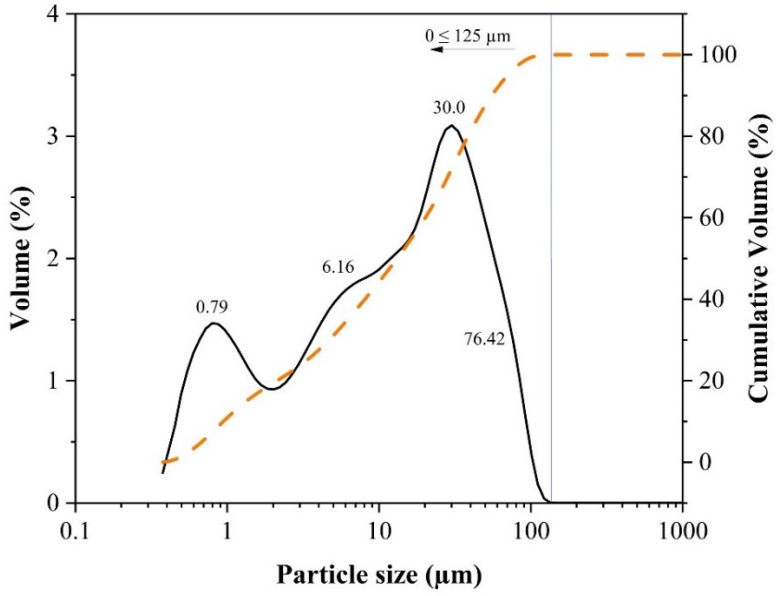

Figure 2. Particle size distribution (PSD) of powdered WBA

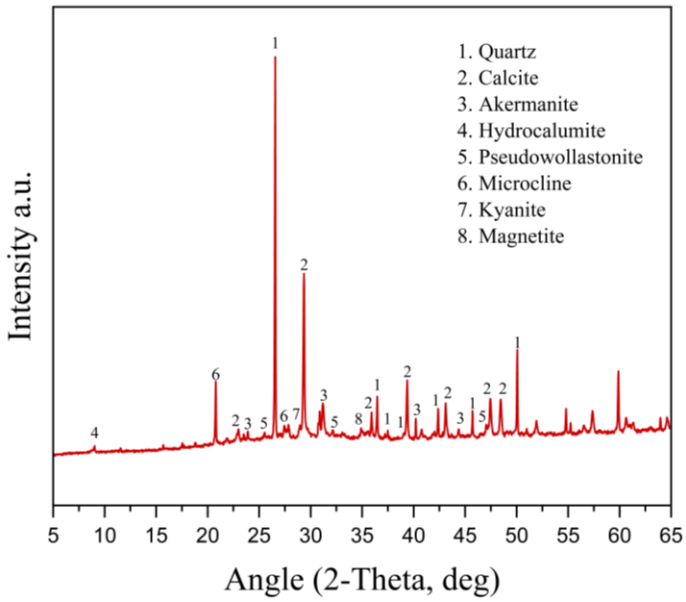

Figure 3. X-ray diffraction (XRD) pattern of powdered WBA

Table 2. Preparation of samples using NaOH:WG combinations with different NaOH molar concentrations

Activator-to-precursor ratio (L/S)	**0.5**															
NaOH:WG ratio	1:1				1:2				1:3				1:4			
NaOH Molar concentrations	4M	6M	8M	10M	4M	6M	8M	10M	4M	6M	8M	10M	4M	6M	8M	10M
Prepared specimens	-	-	-	-	-	-	x	x	-	-	-	-	-	-	-	-
Activator-to-precursor ratio (L/S)	**0.6**															
NaOH:WG ratio	1:1				1:2				1:3				1:4			
NaOH Molar concentrations	4M	6M	8M	10M	4M	6M	8M	10M	4M	6M	8M	10M	4M	6M	8M	10M
Prepared specimens	x	x	x	x	x	x	x	x	x	x	x	x	x	x	x	x
Activator-to-precursor ratio (L/S)	**0.7**															
NaOH:WG ratio	1:1				1:2				1:3				1:4			
NaOH Molar concentrations	4M	6M	8M	10M	4M	6M	8M	10M	4M	6M	8M	10M	4M	6M	8M	10M
Prepared specimens	•	•	•	•	•	•	•	•	•	•	•	•	•	•	•	•

x: Formulations with prepared samples
•: Specimens prepared from formulations with high liquid-to-solid ratios and lower compressive strengths
-: Formulations from which specimens could not be prepared due to rapid reactions during mixing

Using the optimal formulation identified in the first test series (employing the full precursor fraction), specimens were prepared for a second experimental stage. In this stage, the powdered WBA precursor was sieved to obtain three particle-size fractions: ≤ 63 μm, 90-100 μm, and 100-125 μm. Cubic specimens (25 mm) were cast and cured following the same procedure used in the first stage, in which the precursor comprised the entire particle-size distribution. For each fraction, eight specimens were produced; four were tested after 3 days and four after 7 days.

Finally, the precursor fraction that exhibited the highest increase in compressive strength was used to produce a new set of 25 mm cubic specimens. These were tested at 3, 7, and 28 days using the optimal formulation identified in the first stage, together with two additional formulations in which the NaOH:WG ratio and the liquid-to-solid ratio were varied.

2.2 Characterization of alkali-activated binder

In accordance with UNE-EN 196-1, the mechanical behaviour of the AA-WBA pastes was evaluated using an Incotecnic MULTI-R1 Lab-Pre S.L. universal testing machine, operating at a loading rate of 240 $kg \cdot s^{-1}$ with a 2.5 kN load cell. These conditions were maintained throughout the three test stages. Following the mechanical tests, a microstructural analysis of the AA-WBA pastes formulated with different precursor particle sizes was conducted using a JEOL J-7100FE high-resolution scanning electron

microscope (SEM). In addition, the chemical bonds and functional groups of the reaction products were identified and characterised by Fourier transform infrared spectroscopy (FT-IR) within the 4000-450 cm^{-1} spectral range, using a PerkinElmer Spectrum Two™ spectrometer equipped with an ATR accessory, at a resolution of 4 cm^{-1} and four scans per sample. Thermogravimetric analysis (TGA) was also performed to quantify mass variations during controlled heating in a nitrogen (N_2) atmosphere, using a TGA 550 analyser (TA Instruments), at a heating rate of 10 °C·min^{-1} up to a maximum temperature of 1000 °C.

2.3 Determination of environmental impacts

The environmental impact of the concrete used in the proof of concept was assessed, with particular emphasis on the ecotoxicity parameter, in line with European regulations that promote the use of bioassays to evaluate the release of hazardous substances. The luminescence inhibition test using Vibrio fischeri was performed in accordance with ISO 11348-3:2007 [14] as a preliminary assay to detect potential toxic effects in aquatic environments. Leachates were prepared following the UNE-EN 12457-4 [15] leaching procedure, with two replicates per sample. This methodology, supported by recent studies and by the CEN (2022) [16] technical guide on ecotoxicity in construction products, enabled a complementary evaluation of the environmental impacts across the material's life cycle.

2.3.1 Leaching test

Leachates were prepared in accordance with UNE-EN 12457-4, using a compliance test with a liquid-to-solid ratio of 10 L·kg^{-1} to evaluate the release of compounds associated with ecotoxicity under chemical equilibrium conditions. The granular material, with 95% of particles smaller than 10 mm, was maintained in contact with deionised water for 24 hours in a rotary shaker at 10 rpm. The resulting leachates were then vacuum-filtered through a 0.45 µm cellulose nitrate membrane, after which pH and conductivity were measured. The filtered leachates were stored at 4 °C for 24 hours prior to bioassay testing. The specific ionic composition of the leachates, including heavy metals, was determined under the same conditions specified in UNE-EN 12457-2. Analyses were conducted using inductively coupled plasma optical emission spectrometry (ICP-OES) and mass spectrometry (ICP-MS).

2.3.2 Ecotoxicity testing

The ecotoxicological assessment of the proof-of-concept concrete was conducted using a luminescence bioassay with Vibrio fischeri (NRRL B-11177) and Microtox LX® equipment. The bacterial strain was supplied in a lyophilised form and stored at -18 to -20 °C in 1 mL vials. Tests were performed at concentrations of 0, 5.6, 11.25, 22.5, and 45%, with two replicates per concentration, and the pH was adjusted to between 6.5 and 8.5 using HCl.

3 Results and discussion

3.1 Mechanical behaviour

The formulations employed in this study were designated according to a nomenclature that indicates the NaOH-to-WG ratio, the activator-to-precursor (L/S) ratio, and the molar concentration of NaOH. For instance, a designation such as 1:4/0.6/4M refers to a formulation with a NaOH-to-WG ratio of 1:4, an L/S ratio of 0.6 and a NaOH molarity of 4 M.

According to Table 2, the formulations with a L/S ratio of 0.7, although feasible to prepare and yielding highly fluid mixtures, exhibited low compressive strength values. Within this group, the 1:4/0.7/6M formulation achieved the highest strength, reaching 5.65 MPa. The remaining formulations in this trial, which showed even lower values, were excluded from the analysis due to their poor mechanical performance. For the other mixtures within this range, the test specimens disintegrated upon demoulding as a result of insufficient particle cohesion, displaying a distinctly sandy texture.

Conversely, the formulations with a liquid-to-solid ratio of 0.5 reacted very rapidly during mixing, which prevented the preparation of test specimens for compressive strength testing. In contrast, a liquid-to-solid ratio of 0.6 enabled the production of specimens using a fluid and workable mixture. However, it was observed that as the NaOH molar concentration increased, the mixtures became more fluid but induced swelling in the specimens during the first hours of curing. The presence of metallic aluminium generates hydrogen gas during the reaction, leading to expansion of the mixtures [17–20]. Several studies have confirmed that metallic aluminium derived from waste undergoes intense thermal transformation during the incineration process, resulting in the formation of new aluminium-based metallic phases alloyed with other metals and metalloids (Fe, Si, Mn, Ti, Ca), which are responsible for such expansive deformations in the specimens [18]

Table 3 summarises the highest compressive strength results obtained for formulations prepared with a L/S ratio of 0.6, using the full precursor fraction. The reported range, from 1:3/0.6/4M to 1:4/0.6/10M corresponds to the combination that delivered the best compressive performance. Among these, the 1:4/0.6/4M formulation exhibited the highest mechanical performance, reaching a compressive strength of 11.16 MPa. For this formulation, the activator's SiO_2/Na_2O ratio was 2.7. Within the group of formulations with the highest mechanical performance, the activator modulus varied between 1.89 and 2.7

Table 3. Compressive strength results for all precursor particle sizes

Activator-to-precursor ratio (L/S)	**0.6**							
NaOH:WG ratio	1:3				**1:4**			
NaOH Molar concentrations	4M	6M	8M	10M	**4M**	6M	8M	10M
28-day compressive strength (MPa)	10.86	9.76	4.28	2.76	11.16	9	9.65	5.31
SiO_2/Na_2O activator module	2.52	2.23	2.03	1.89	2.70	2.46	2.26	2.13
Ratio a/c total sample*	0.34	0.33	0.32	0.31	0.33	0.32	0.31	0.31

*: Total sample ratio without the solid fraction contained in the activator (Si, Na from WG and NaOH)

This finding is particularly relevant as it highlights that deviations from standard formulations reported in previous studies can substantially affect compressive strength. Several authors have observed that an activator modulus exceeding 2 may adversely impact both the workability and the mechanical performance of the material [21,22]. Other studies [12], however, have demostrated that this modulus is not the sole parameter influencing strength and workability at an industrial scale. Increasing the proportion of NaOH in the alkaline activating mixture enhances the reactivity with the metallic aluminium present in WBA, which promotes hydrogen generation and, consequently, reduces the mechanical performance. Nevertheless, research on paste formulations has shown that an appropriate balance between high compressive strength and adequate workability can be achieved. Furthermore, both properties can be further optimized through the incorporation of mineral and chemical additives that improve mixture handling, facilitating the production of street furniture and outdoor paving elements.

Based on the results obtained for the best-performing formulation in the first testing stage, in which specimens with a 1:4/0.6/4M ratio exhibited the highest compressive strength, the corresponding mixtures for the second stage were prepared. However, formulations incorporating particles smaller than 63 µm could not be produced, as the mixtures underwent an accelerated reaction during mixing, leading to premature setting. In contrast, mixtures with particle sizes between 90-100 µm and 100-125 µm produced the results shown in Figure 4a, where the formulations containing 90-100 µm particles and the optimal mixture displayed superior mechanical performance. Nevertheless, when the NaOH:WG ratio was adjusted to 1:2 while using a NaOH molar concentration of 6 M, no favourable results were obtained. For the 100-125 µm particle-size fraction, although specimen fabrication was possible, the samples exhibited substantial porosity, which negatively affected their compressive strength.

In the third testing stage, the optimal formulation (1:4/0.6/4M), combined with the most suitable particle-size fraction (90-100 µm), was selected as the reference for preparing new specimens with comparable mixtures. In these formulations, slight adjustments were introduced to the NaOH:WG ratio and the L/S ratio in order to assess potential variations in both compressive strength and workability. Figure 4b confirms that the previously identified optimal formulation (1:4/0.6/4M), incorporating precursor particles in the 90-100 µm range, delivers the highest compressive strength for this material, reaching values of up to 23.5 MPa.

3.2 Physicochemical characterization

3.2.1 Thermogravimetric (TGA) analysis

Figure 5 presents the thermogravimetric analysis (TGA) results and the corresponding derivative curves (DTG) for the powdered WBA precursor and for the two AA-WBA formulations produced using the two particle-size fractions (90-100 µm and 100-125 µm).

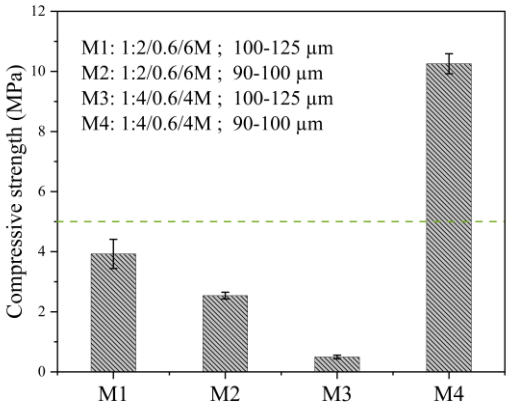

Fig. 4a

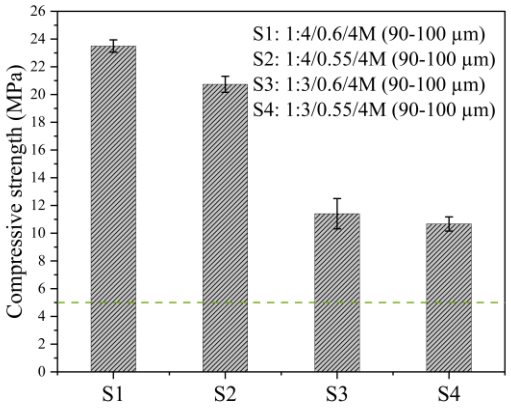

Fig. 4b

Figure 4. a) Compressive strength at 7 days of samples with different particle sizes. b) Compressive strength at 28 days with precursor particle size between 90-100 µm

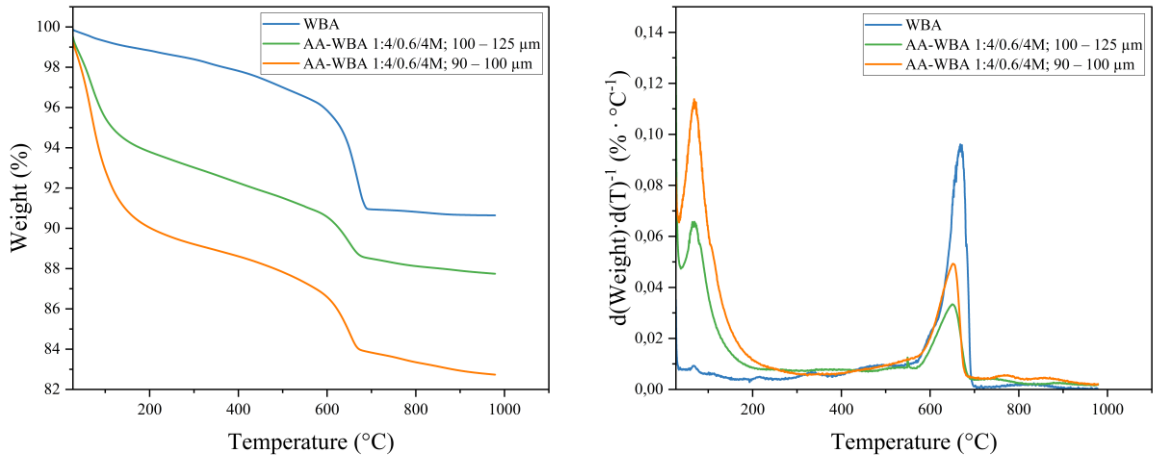

Figure 5. TGA and DTG curves of powdered WBA samples and formulations with higher mechanical strength

In the range of 25-200 °C, all samples exhibit a mass loss associated with the release of physically adsorbed water and structurally bound water. This loss is more pronounced in the AA-WBA formulations (90-100 µm and 100-125 µm) than in the WBA precursor, indicating the formation of hydrated products during the alkaline activation process. The most prominent peaks in the DTG curves, occurring between 110 and 150 °C, are attributed to the dehydration of C-(A)-S-H and/or N-A-S-H gels, consistent with previous findings reported in the literature [23–25].

In the range of 200-400 °C, low-intensity secondary peaks are observed in the activated formulations, which may be associated with the dehydroxylation of hydrotalcite-type phases or hydrated aluminates. In contrast, the powdered WBA precursor shows no significant variations within this interval, confirming its predominantly anhydrous nature. Between 400 and 700 °C, the activated formulations display additional mass losses attributable to the decomposition of carbonates formed on the particle surfaces. The powdered WBA precursor, by comparison, exhibits a pronounced DTG peak around 650-700 °C, corresponding to the thermal decomposition of calcium carbonate ($CaCO_3$) present in the original material. This behaviour has been previously reported in studies on alkali-activated incineration residues [26,27].

Above 700 °C, all three samples reach a thermally stable region, with no further significant mass loss. The total mass loss up to 1000 °C is approximately 10% for the powdered WBA precursor and between 12% and 14% for the activated formulations, reflecting the higher content of structural water and hydrated phases in the alkaline systems.

Comparatively, the formulation with a particle fraction of 90-100 µm exhibits a more pronounced initial weight loss and a more stable thermal response at elevated temperatures, suggesting a higher degree of reaction and the formation of a denser gel network. This behaviour is consistent with its superior mechanical performance, as a more developed and homogeneous microstructure promotes both the compressive strength and the thermal stability of the final material [28].

3.2.2 Fourier transform infrared (FT-IR) analysis

Figure 6 presents the FT-IR spectra of the powdered WBA and the two alkali-activated formulations (AA-WBA 90-100 µm and AA-WBA 100-125 µm), which exhibit comparable families of bands, albeit with variations in intensity and position that reflect differences in composition and degree of hydration. In the 3400-1650 cm^{-1} region, associated with the stretching and bending vibrations of -OH groups from adsorbed or structural water, the AA-WBA formulations show broader and more intense bands than the precursor (WBA). This behaviour indicates the presence of bound water within the hydrated gels formed during alkali activation. These signals are consistent with the mass loss observed in the TGA analysis below 200 °C, confirming the presence of both free and structural water in the samples [29,30].

The main bands, attributed to the asymmetric Si-O-(Si/Al) stretching vibrations characteristic of C-(A)-S-H and/or N-A-S-H reaction gels, appear in the 1050-980 cm^{-1} region. Variations in the position and width of this band among the samples indicate differences in the degree of polymerisation and in the Si/Al ratio of the reaction products. The WBA sample exhibits a more defined signal at 1016 cm^{-1}, whereas the AA-WBA samples show slight shifts and band broadening, consistent with the development of a more amorphous network typical of alkali-activated materials [25,31]. These features confirm the formation of gel phases associated with the activation process.

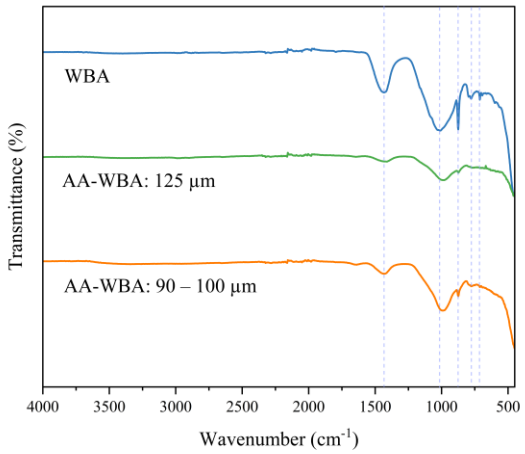

Figure 6. FT-IR spectra of powdered WBA and formulations showing enhanced mechanical performance

The characteristic carbonate bands (1420-1433 cm^{-1} and 870-875 cm^{-1}) are observed in all three samples, although they appear with greater intensity in the AA-WBA (90-100 µm) formulation. This trend aligns with the TGA/DTG results, in which this sample exhibits the most pronounced mass loss between 500 and 800 °C and a maximum decomposition peak at approximately 600-700 °C, corresponding to the thermal decomposition of carbonates ($CaCO_3 \rightarrow CaO + CO_2$). Taken together, these findings indicate a higher carbonate content, or a greater extent of carbonation, in the AA-WBA (90-100 µm) formulation [29,30].

The correlation between the FT-IR and TGA/DTG analyses indicates that the AA-WBA (90-100 µm) formulation exhibits a higher degree of carbonation, as well as distinct variations in the Si-O region that reflect differences in gel polymerization [32]. Overall, the findings demonstrate that particle size and formulation exert a direct influence on carbonation and on the development of C-(A)-S-H and/or N-A-S-H gels.

3.2.3 Scanning electron microscopy (SEM) analysis

Figure 7 presents SEM micrographs of the AA-WBA material acquired using a low-energy secondary electron detector. Images (a) and (b), corresponding to the formulation with a particle size fraction of 100-125 µm, demonstrate that particle size plays a critical role in the resulting microstructure and degree of reaction.

A heterogeneous microstructure is observed, characterised by highly porous regions and the presence of partially dissolved particles remaining after alkali activation. This indicates an incomplete reaction, likely associated with the lower reactivity of the larger particles, possibly due to their glassy nature and the presence of inert oxides. Consequently, voids (pores) are generated between particles that were not fully encapsulated by the reaction gel, a phenomenon that may be exacerbated by hydrogen release from residual metallic aluminium [18].

At a larger scale (Figure 7b), compact and laminar textures can be observed, which are characteristic of C-A-S-H gels and appear to have formed superficially on the

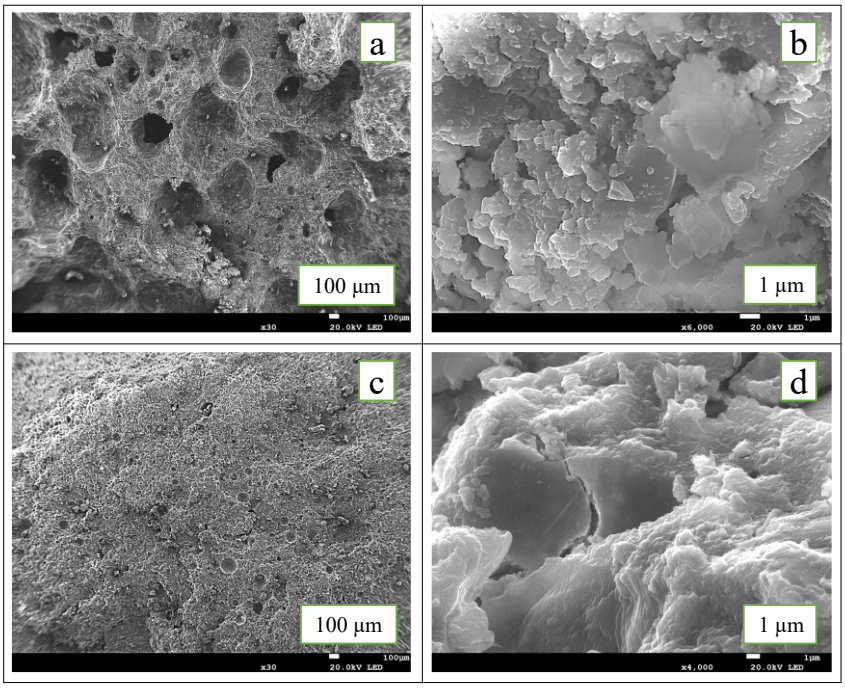

Figure 7. SEM micrographs of AA-WBA samples: a y b) Samples with precursor particle size 125 µm; c y d) Samples with precursor particle size 90-100 µm

unreacted coarse particles. In this material, the predominant formation of C-A-S-H gels is consistent with the high CaO and Al_2O_3 contents of the slag. Nonetheless, the presence of Na_2O derived both from the sodium silicate activator and from the slag itself suggests the possible coexistence of N-A-S-H phases.

Micrographs (c) and (d), in contrast with the previous images, reveal a more homogeneous and compact microstructure with markedly reduced porosity, indicating a more efficient alkali-activation reaction. This improvement is associated with a more complete dissolution of the precursor particles and the more abundant and continuous formation of the C-A-S-H and/or N-A-S-H binding gels, which correlates with the enhanced mechanical performance of the material. At a larger scale (Figure 7d), a dense and continuous matrix is observed, in which most particles are fully incorporated into the gel phase, demonstrating a more advanced reaction and greater microstructural consolidation.

3.3 Proof of concept

To promote progress within a standardised evaluation framework that assesses the maturity of research, from the conceptual stage to full-scale implementation under real conditions, while considering Technology Readiness Levels (TRL), a proof of concept was undertaken. This approach supports innovation by bridging the transition from laboratory-based conceptual development to practical application, thereby linking theoretical principles with operational performance [13].

To validate the concept, a prototype cover for an inspectable box used in paving was manufactured in collaboration with Escofet by Molins, a world-renowned Barcelona-based company specialising in the design and production of street furniture, paving elements and architectural concrete for public spaces and buildings (Figure 8). The alkali-activated binder was produced using the optimal formulation identified in this study (AA-WBA 1:4/0.6/4M; 90-100 µm), together with the granitic and calcareous aggregates routinely employed by Escofet by Molins in their architectural concrete. The mixture proportions are presented in Table 4. These proportions are based on an appropriate mix design (Fuller–Thompson method), in accordance with the particle size distribution of the available aggregates, as used by Escofet by Molins in its precast elements. The mixture was prepared at the Escofet industrial plant using a vertical-shaft (planetary) mixer with a capacity of 0.33 m³ per batch (cycle). The dosage of the aggregates was defined as a percentage of the total weight of the sample; in this preliminary test, a 15 kg sample was prepared, which was used to manufacture the proof of concept and several specimens for the control of mechanical behaviour. The resulting concrete displayed a highly compact structure, with a uniform distribution of aggregates within the alkali-activated matrix and excellent overall homogeneity (Figure 9). Strong aggregate-matrix bonding was observed, contributing to the structural integrity and durability of the material. After 28 days of outdoor curing (at

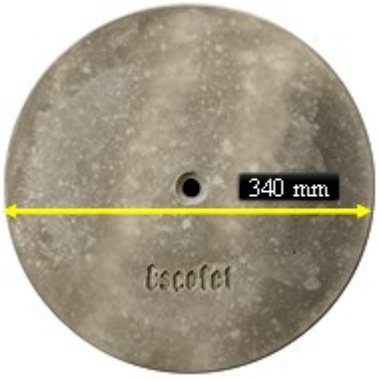

Figure 8. Cover for inspection box in outdoor paving formulated from alkali-activated binder using WBA as the sole precursor

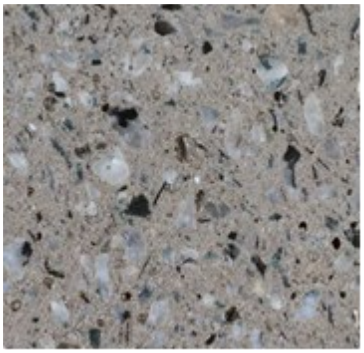

Figure 9. Cross-sectional image of the inspection box cover in concrete formulated for the proof of concept

the Escofet facilities), the prototype was cut into twelve test specimens with average dimensions of 44×44×42 mm for compressive testing. The samples reached an average compressive strength of 14 MPa, meeting the performance requirements for urban pedestrian paving applications.

Proof-of-concept studies from previous research [13] have highlighted that, although initial trials yield promising results, scalability remains a significant challenge. Technical feasibility is largely dependent on production volumes: increasing the liquid content in the mixtures can reduce mechanical performance, affect workability, and necessitate construction methods different from those employed in the production of Portland cement-based components. Moreover, specific production conditions are required in terms of both labour and equipment. Further research is therefore needed on the use of tailored additives and alternative curing strategies to adapt the casting process for pilot- and industrial-scale production.

3.4 Environmental characterization

Figure 10 presents the dose-response curve for the concrete sample developed in the proof-of-concept study. The luminescence inhibition values represent the average of two replicates of the same sample, with the differences between replicates indicated by error bars. The results demonstrate good reproducibility between replicates. The bacterial luminescence response at the two contact times assessed, 15 and 30 minutes, showed no significant differences. Ecotoxicity was evaluated in accordance with technical report CEN/TS 17459 [16], which specifies that the lowest ineffective dilution (LID), defined as the highest dilution causing the least significant effect on the test organism, must not exceed 8. This parameter is calculated based on the EC_{20} value, corresponding to the leachate concentration that induces a 20% reduction in luminescence, as expressed by the following equation:

$$LID = \frac{1}{\left(\frac{EC_{20}}{100}\right)}$$

Table 4. Material dosing for AA-WBA concrete used in the production of pavement manhole covers

Aggregates	
Arid calcareous 1-3 mm	3750 g
Granitic arid 2-6.3 mm	2143 g
Small granite aggregate 4-12.5 mm	4821 g
Alkali-Activated Binder (AA-WBA) - 1:4/0,6/4M	
WBA (precursor)	4286 g
Sodium silicate (Na_2SiO_3)	2057 g
Sodium hydroxide (NaOH) - 4M	514 g

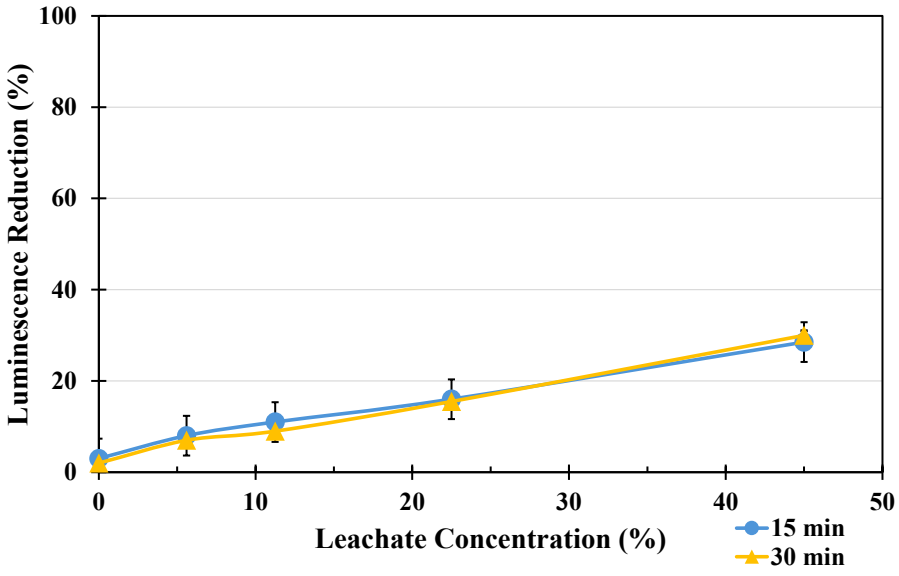

Figure 10. Percentage reduction in luminescence of the concrete samples after 15 and 30 minutes in the proof-of-concept test

For the concrete produced in the proof-of-concept study, the leachate concentration (EC_{20}) was 28.40, corresponding to an LID value of 3.52. This value does not exceed the established limit, indicating that the effect of powdered WBA on bacterial luminescence is reduced following its incorporation into the concrete with the formulated AA-WBA binder.

Table 5. pH and conductivity values of the precursor (powdered WBA) and the concrete in the proof-of-concept test

Specimen	pH	Conductivity ($mS \cdot cm^{-1}$)
WBA	9.89 ± 0.06	2.14 ± 0.04
Proof-of-concept concrete	10.36 ± 0.03	3.09 ± 0.98

Table 5 presents the pH and conductivity values of the leachates from the powdered WBA samples (precursor) and the concrete developed in the proof-of-concept study. The results correspond to two replicates, with their respective standard deviations. The measured conductivity values are consistent with the pH of each sample, reflecting the presence of dissolved ions in the leachate. In the alkali-activated concrete (proof-of-concept specimen), no significant changes in leachate pH were observed. These results indicate that the concrete has reached a stabilized phase of ion release, meaning it is no longer undergoing rapid leaching while still exhibiting residual chemical activity. This suggests a reduced risk of generating highly alkaline or ion-rich leachates that could affect receiving waters or soils and demonstrates effective retention and immobilization of alkaline elements, which is a critical consideration when incorporating incineration residues that may contain mobile components.

The results of the specific ionic composition analysis of the leachates (heavy metals) are presented in Table 6. Both the precursor (powdered WBA) and the proof-of-concept concrete exhibit concentrations of most leached metals and metalloids well below the limit for acceptance at landfills as inert waste [33]. For Mo, Sb, and As, the values fall within the thresholds defined for non-hazardous waste. These findings indicate low mobility of potentially hazardous elements and confirm both the environmental safety of the material and its suitability for use in the production of concrete elements.

4 Conclusions

The results demonstrate that it is technically feasible to formulate an alkali-activated binder using bottom ash from municipal solid waste incineration (WBA) as the sole precursor. The identified optimal formulation (1:4/0.6/4 M; 90-100 µm) developed a dense microstructure characterised by the coexistence of C-(A)-S-H and N-A-S-H gels, enabling the attainment of competitive compressive strengths. The proof-of-concept concrete reached values of up to 14 MPa, which are suitable for non-structural urban applications.

In comparison with the compressive strengths achieved by the binder (AA-WBA 1:4/0.6/4M, 90-100 µm) under laboratory conditions, the mechanical performance of the proof-of-concept concrete could be further enhanced by adopting manufacturing practices specific to alkali-activated cements. These include the optimisation of mixing protocols, curing regimes, equipment cleaning procedures, control of initial moisture levels, material pre-conditioning, and a work culture adapted to the distinct requirements of alkali-activated systems, which differ from those typically applied to Portland cement-based concretes.

The study demonstrates that the particle-size distribution of the precursor is a critical factor governing the efficiency of alkaline activation. Fractions in the 90-100 µm range produced a higher degree of reaction, lower porosity, and a more cohesive matrix, whereas finer particles (≤63 µm) induced accelerated and uncontrolled reactions, and coarser particles (100-125 µm) resulted in more porous microstructures with limited reactivity. Similarly, the NaOH:WG ratio and the SiO_2/Na_2O modulus exerted a marked influence on both workability and mechanical strength, underscoring the need for precise chemical balance to ensure material stability and performance.

Leaching tests, ecotoxicity assessments, and ionic analyses confirmed that both the WBA and the formulated concrete exhibit low heavy metal mobility, conlying whtit the limits for inert waste for most metal and metalloid, and with non-hazardous waste criteria for Mo, Sb and As. The AA-WBA-based concrete displayed an LID value below the recommended threshold, indicating the absence of significant toxic effects. These results confirm the environmental safety of the material and underscore its potential to contribute to closing material cycles within circular economy frameworks, promoting the use of municipal waste in low-impact urban applications.

Table 6. Leached metal concentrations from the precursor (powdered WBA) and the proof-of-concept concrete, compared with the permissible limit values for landfill acceptance according to regulatory thresholds [33]

mg/kg (ppm)	Zn	Cr	Mo	Ni	Cu	Sb	As	Pb	Cd	Hg	Ba	Se
WBA (precursor)	0.09	0.08	0.86	0.02	1.30	0.34	0.00	0.00	0.00	0.00	0.36	0.02
Concept proof concrete	0.18	0.09	0.41	0.02	0.64	0.68	1.00	0.34	0.00	0.00	0.08	0.08
Inert waste	4	0.5	0.5	0.4	2	0.06	0.5	0.5	0.04	0.01	20	0.1
Non-hazardous waste	50	10	10	10	50	0.7	2	10	1	0.2	100	0.5
Hazardous waste	200	70	30	40	100	5	25	50	5	2	300	70

Acknowledgements

The authors wish to thank Escofet by Molins for providing materials, personnel, equipment, and facilities for the proof-of-concept study; the DIOPMA research group at the University of Barcelona and CCiTUB for access to equipment, laboratory supplies, and for conducting the TGA, FT-IR, and SEM analyses; and the Department of Chemistry and Process and Resource Engineering (QUIPRE) at the University of Cantabria for their support with the Microtox® measurements. The authors acknowledge the support of the COST Action CircularB-Implementation of a Circular Economy in the Built Environment. Mr Fabian Cuspoca gratefully acknowledges the Secretariat of Universities and Research of the Department of Business and Knowledge of the Generalitat of Catalonia and the European Social Fund Plus (ESF+) for the FI-SDUR 2024 research scholarship.

Funding

This work was partially supported by Programa Iberoamericano de Ciencia y Tecnología para el Desarrollo (CYTED) through Rede ECoEICo, and by Grant ACE051/22/000011 funded by ACCIÓ, the Catalan Government's Agency for Business Competitiveness. The Catalan Government also supported this work through Grant 2021 SGR 00708, managed by the Agency for Management of University and Research Grants (AGAUR). DIOPMA research group is recognized as a TECNIO-certified technology developer by the Government of Catalonia..

CRediT authorship contribution statement

Fabian Cuspoca: Data Curation, Formal Analysis, Investigation, Methodology, Validation, Writing-Original Draft Preparation. **Jofre Mañosa**: Validation, Writing-Review and Editing. **Joan Ramon Rosell**: Methodology, Supervision, Writing-Review and Editing. **Gerard Faneca**: Funding Acquisition, Resource, Writing-Review and Editing. **Josep Maria Chimenos**: Conceptualization, Funding Acquisition, Methodology, Supervision, Writing-Review and Editing. All authors have read and agreed to the published version of the manuscript.

Declaration of competing interest

The authors declare that the research was conducted in the absence of any commercial or financial relationships that could be construed as a potential conflict of interest.

Abbreviations

This manuscript uses the following abbreviations:

AA-WBA	Bottom ash-based alkali-activated material
C-A-S-H	Calcium–aluminium–silicate–hydrate
FT-IR	Fourier Transform Infrared Spectroscopy
LID	Lowest Ineffective Dilution
LOI	Loss on ignition
N-A-S-H	Sodium–aluminium–silicate–hydrate
OPC	Ordinary Portland Cement
SEM	Scanning Electron Microscopy
TGA	Thermogravimetric Analysis
WBA	Waste-incineration bottom ash (precursor)
wt. (%)	Weight percent

References

[1] B. Chen, M. Brito van Zijl, A. Keulen, G. Ye, Thermal Treatment on MSWI Bottom Ash for the Utilisation in Alkali Activated Materials, KnE Engineering 2020 (2020) 25–35. https://doi.org/10.18502/keg.v5i4.6792.

[2] P.C.D. Tortora, A. Maldonado-Alameda, J. Mañosa, A.C. Quintero-Payan, C. Leonelli, I. Lancellotti, J.M. Chimenos, Effect of Temperature and Humidity on the Synthesis of Alkali-Activated Binders Based on Bottom Ash from Municipal Waste Incineration, Sustainability 14 (2022) 1848. https://doi.org/10.3390/su14031848.

[3] A. Maldonado-Alameda, J. Giro-Paloma, A. Svobodova-Sedlackova, J. Formosa, J.M. Chimenos, Municipal solid waste incineration bottom ash as alkali-activated cement precursor depending on particle size, J Clean Prod 242 (2020). https://doi.org/10.1016/j.jclepro.2019.118443.

[4] A. Maldonado-Alameda, J. Giro-Paloma, A. Alfocea-Roig, J. Formosa, J.M. Chimenos, Municipal Solid Waste Incineration Bottom Ash as Sole Precursor in the Alkali-Activated Binder Formulation, Applied Sciences 10 (2020) 4129. https://doi.org/10.3390/app10124129.

[5] X.C. Qiao, M. Tyrer, C.S. Poon, C.R. Cheeseman, Characterization of alkali-activated thermally treated incinerator bottom ash, Waste Management 28 (2008) 1955–1962. https://doi.org/10.1016/j.wasman.2007.09.007.

[6] N. Yamaguchi, M. Nagaishi, K. Kisu, Y. Nakamura, K. Ikeda, Preparation of monolithic geopolymer materials from urban waste incineration slags, Journal of the Ceramic Society of Japan 121 (2013) 847–854. https://doi.org/10.2109/jcersj2.121.847.

[7] J. Giro-Paloma, A. Maldonado-Alameda, J. Formosa, L. Barbieri, J.M. Chimenos, I. Lancellotti, Geopolymers based on the valorization of Municipal Solid Waste Incineration residues, in: IOP Conf Ser Mater Sci Eng, 2017. https://doi.org/10.1088/1757-899X/251/1/012125.

[8] J.M. Chimenos, M. Segarra, M.A. Fernández, F. Espiell, Characterization of the bottom ash in municipal solid waste incinerator, J Hazard Mater 64 (1999) 211–222. https://doi.org/10.1016/S0304-3894(98)00246-5.

[9] B.S. Bandarra, J.L. Pereira, R.C. Martins, A. Maldonado-Alameda, J.M. Chimenos, M.J. Quina, Opportunities and Barriers for Valorizing Waste Incineration Bottom Ash: Iberian Countries as a Case Study, Applied Sciences 2021, Vol. 11, Page 9690 11 (2021) 9690. https://doi.org/10.3390/APP11209690.

[10] D. Blasenbauer, F. Huber, J. Lederer, M.J.M.J. Quina, D. Blanc-Biscarat, A. Bogush, E. Bontempi, J. Blondeau, J.M.J.M. Chimenos, H. Dahlbo, J. Fagerqvist, J. Giro-Paloma, O. Hjelmar, J. Hyks, J. Keaney, M. Lupsea-Toader, C.J.C.J. O'Caollai, K. Orupõld, T. Pająk, F.-G.F.-G. Simon, L. Svecova, M. Šyc, R. Ulvang, K. Vaajasaari, J. Van Caneghem, A. van Zomeren, S. Vasarevičius, K. Wégner, J. Fellner, Legal situation and current practice of waste incineration bottom ash utilisation in Europe, Waste Management 102 (2020) 868–883. https://doi.org/https://doi.org/10.1016/j.wasman.2019.11.031.

[11] R. del Valle-Zermeño, J. Gómez-Manrique, J. Giro-Paloma, J. Formosa, J.M. Chimenos, Material characterization of the MSWI bottom ash as a function of particle size. Effects of glass recycling over time, Science of The Total Environment 581–582 (2017) 897–905. https://doi.org/10.1016/j.scitotenv.2017.01.047.

[12] A. Maldonado-Alameda, J. Giro-Paloma, J. Mañosa, J. Formosa, J.M.J.M. Chimenos, Alkali-activated binders based on the coarse fraction of municipal solid waste incineration bottom ash, Bol Soc. Esp. Ceram. Vidr. In press (2020) 313–324.

[13] J.M. Chimenos, F. Cuspoca, A. Maldonado-Alameda, J. Mañosa, J.R. Rosell, A. Andrés, G. Faneca, L.F. Cabeza, MSW Incineration Bottom Ash-Based Alkali-Activated Binders as an Eco-Efficient Alternative for Urban Furniture and Paving: Closing the Loop Towards Sustainable Construction Solutions, Buildings 15 (2025) 1–24. https://doi.org/10.3390/buildings15091571.

[14] ISO, ISO 11348-3:2007 - Water quality - Determination of the inhibitory effect of water samples on the light emission of Vibrio fischeri (Luminescent bacteria test) -- Part 3: Method using freeze-dried bacteria, ISO/TC 147/SC5 - Water Quality/Biological Methods (2018) 21 pp. http://www.iso.org/iso/home/store/catalogue_ics/catalogue_detail_ics.htm?csnumber=40518.

[15] European Committee for Standarization, EN 12457-4: Compliance test for leaching of granular waste materials and sludges. Part 4: One stage batch test at a liquid to solid ratio of 10 l/kg for materials with particle size below 10 mm (without or with size reduction)., (2002).

[16] European Committee for Standardization (CEN), CEN/TS 17459:2024 EX Construction products: Assessment of release of dangerous substances - Determination of ecotoxicity of construction product eluates, Madrid, 2024.

[17] X. Tian, F. Rao, C.A. León-Patiño, S. Song, Effects of aluminum on the expansion and microstructure of alkali-activated MSWI fly ash-based pastes, Chemosphere 240 (2020) 124986. https://doi.org/10.1016/j.chemosphere.2019.124986.

[18] A. Saffarzadeh, N. Arumugam, T. Shimaoka, Aluminum and aluminum alloys in municipal solid waste incineration (MSWI) bottom ash : A potential source for the production of hydrogen gas, Int J Hydrogen Energy 41 (2015) 820–831. https://doi.org/10.1016/j.ijhydene.2015.11.059.

[19] J.E. Aubert, B. Husson, A. Vaquier, Metallic aluminum in MSWI fly ash: quantification and influence on the properties of cement-based products, Waste Management 24 (2004) 589–596. https://doi.org/10.1016/j.wasman.2004.01.005.

[20] S.K. Adhikary, T. Luukkonen, M.A.H. Bhuyan, Y. Yu, P. Perumal, A method of pretreating incineration ashes containing metallic aluminium using NaOH to mitigate volume expansion under highly alkaline conditions, Constr Build Mater 450 (2024) 138639. https://doi.org/10.1016/j.conbuildmat.2024.138639.

[21] X. Ouyang, Y. Ma, Z. Liu, J. Liang, G. Ye, Effect of the Sodium Silicate Modulus and Slag Content on Fresh and Hardened Properties of Alkali-Activated Fly Ash/Slag, Minerals 10 (2019) 15. https://doi.org/10.3390/min10010015.

[22] S. Choi, K.M. Lee, Influence of Na_2O content and Ms (SiO_2/NamO) of alkaline activator on workability and setting of alkali-activated slag paste, Materials 12 (2019). https://doi.org/10.3390/ma12132072.

[23] C.K. Yip, G.C. Lukey, J.S.J. van Deventer, The coexistence of geopolymeric gel and calcium silicate hydrate at the early stage of alkaline activation, Cem Concr Res 35 (2005) 1688–1697. https://doi.org/10.1016/j.cemconres.2004.10.042.

[24] B. Pacewska, I. Wilińska, Comparative investigations of influence of chemical admixtures on pozzolanic and hydraulic activities of fly ash with the use of thermal analysis and infrared spectroscopy, J Therm Anal Calorim 120 (2015) 119–127. https://doi.org/10.1007/s10973-014-4334-x.

[25] J.L. Provis, S.A. Bernal, Geopolymers and Related Alkali-Activated Materials, Annu Rev Mater Res 44 (2014) 299–327. https://doi.org/10.1146/annurev-matsci-070813-113515.

[26] S. Kucharczyk, W. Pichór, The effect of waste-expanded perlite on alkali activation of ground granulated blast furnace slag, Mater Struct 56 (2023) 58. https://doi.org/10.1617/s11527-023-02150-8.

[27] S.A. Walling, S.A. Bernal, L.J. Gardner, H. Kinoshita, J.L. Provis, Blast furnace slag-$Mg(OH)_2$ cements activated by sodium carbonate, RSC Adv 8 (2018) 23101–23118. https://doi.org/10.1039/C8RA03717E.

[28] C. Li, H. Sun, L. Li, A review: The comparison between alkali-activated slag (Si + Ca) and metakaolin (Si + Al) cements, Cem Concr Res 40 (2010) 1341–1349. https://doi.org/10.1016/j.cemconres.2010.03.020.

[29] A. Sujak, M. Pyzalski, K. Durczak, T. Brylewski, P. Murzyn, K. Pilarski, Studies on Cement Pastes Exposed to Water and Solutions of Biological Waste, Materials 15 (2022) 1931. https://doi.org/10.3390/ma15051931.

[30] S.J. Kemp, A.L. Lewis, J.C. Rushton, Detection and quantification of low levels of carbonate mineral species using thermogravimetric-mass spectrometry to validate CO2 drawdown via enhanced rock weathering, Applied Geochemistry 146 (2022) 105465. https://doi.org/10.1016/j.apgeochem.2022.105465.

[31] M.O. Yusuf, Bond Characterization in Cementitious Material Binders Using Fourier-Transform Infrared Spectroscopy, Applied Sciences 13 (2023) 3353. https://doi.org/10.3390/app13053353.

[32] C. Marieta, A. Martín-Garin, I. Leon, A. Guerrero, Municipal Solid Waste Incineration Fly Ash: From Waste to Cement Manufacturing Resource, Materials 16 (2023) 2538. https://doi.org/10.3390/ma16062538.

[33] Council of the European Union, 2003/33/EC, Council Decision establishing criteria and procedures for the acceptance of waste at landfills pursuant to Article 16 of and Annex II to Directive 1999/31/EC, Official Journal of the European Communities (2003) 27–49.